Acquisition Correction and Reconstruction for a Clinical SPECT/MRI Insert

Ashley J. Morahan, Kjell Erlandsson, Ilenia D'Adda, Marco Carminati, Annarita Savi, Rosa-Maria Moresco, Kalman Nagy, Zoltan Nyitrai, Botond Tolgyesi, Debora Salvado, Pieter Van Mullekom, Carlo E. Fiorini, Brian F. Hutton

Abstract–**The development of the first clinical simultaneous Single Photon Emission Computed Tomography (SPECT) and Magnetic Resonance Imaging (MRI) system was carried out within the INSERT project. The INSERT scanner was constructed under the initial project, but its performance was not fully evaluated; here we have reconstructed the first images on the SPECT system. Calibration and acquisition protocols were developed and used to establish the clinical feasibility of the system. The image reconstruction procedures were implemented on the first phantom images in order to assess the system's imaging capabilities. This study solved issues involving incomplete data sets and pixel failure in the prototype detector system. The final images determined a measure of trans-axial image resolution, giving average values of 9.14 mm and 6.75 mm in the radial and tangential directions respectively. The work carried out on the complete system produced several clinical phantom images which utilized the capabilities of both SPECT and MRI.**

I. INTRODUCTION

INSERT is the world's first clinical simultaneous SPECT/MRI system. The system is a brain SPECT insert, designed for complete integration with any clinical MRI system. The stationary insert system is composed of a partial ring of 20 detector units, each with a 10x5 cm^2 CsI(TI) crystal, silicon photomultiplier (SiPM) and ASIC readout. A novel MR compatible collimator; the multi-mini-slit-slat (MSS), [1], was designed specifically for the compatibility and clinical needs of the system. The use of the MSS collimator requires the implementation of a specific calibration procedure, which was established on a single detector system, [2], and initially tested on a semi-operational system, [3].

The partial ring MSS collimator imposes some limitations on the system's sampling. In this work we utilise a dual reconstruction technique in order to improve angular sampling of the system. Due to hardware issues we had cases of detection failure in which data were missing across a few affected units. The calibration and event reconstruction techniques were found to provide a means of correcting missing event data. The limitations of the prototype were overcome by the calibration procedure, producing successful reconstructed phantom images, which were further improved by the dual acquisition protocol.

II. METHODS

A. Event Reconstruction

The system carries out event reconstruction with a maximum likelihood (ML) algorithm. The ML reconstruction requires modelling of each SiPM Light Response Function (LRF). LRF models were constructed for each detector channel, derived from a uniformity flood acquisition, [4]. LRF modelling has previously been used to evaluate the detectors, [5]; here we establish use of the models as a correction for hardware failure. The LRF can account for missing event data in a given channel by modelling the known spatial response and interpolating counts from surrounding channels. This method is limited to small regions as it cannot correct large areas of missing data.

B. System Calibration

The calibration procedure involves two steps; detector calibration and system calibration. The detector calibration involved standard linearity and uniformity corrections of the projection data. The linearity and uniformity corrections were carried out with simple transformations of the projection data using a flood source and linearity collimators. The system calibration consists of a geometric and sensitivity calibration followed by event re-sampling; this procedure accounts for the MSS system design. The geometric calibration has been established previously, [2]. The sensitivity calibration required data with a planar phantom, filled with 50 MBq of ^{99m}Tc solution, and placed close to each of the collimated detectors. The sensitivity profiles were fitted using equation (1), where φ is the sampling angle, $G_\sigma(\varphi)$ is a Gaussian function and the summation is done over all mini-slits i for each collimator section j.

$$S_j(\phi) = \sum_i G_\sigma(\phi) * A_{i,j} \cos^p \phi + b_j \quad (1)$$

A.J. Morahan, K. Erlandsson, D. Salvado and B.F. Hutton are with Institute of Nuclear Medicine, University College London, London NW1 2BU, UK (contact: ashley.morahan.17@ucl.ac.uk).

I. D'Adda, M. Carminati and C.E. Fiorini, are with Dipartimento di Elettronica, Informazione e Bioingegneria, Politecnico di Milano and INFN Sez. Milano, Italy.

A. Savi and R.-M. Moresco are with Ospedale San Raffaele, Milano, via Olgettina 60, 20132 Milano, Italy

K. Nagy, Z. Nyitrai and B. Tolgyesi are with MEDISO Ltd, Budapest, 1037 Hungary.

P. Van Mullekom is with Nuclear Fields, 5827 AP Vortum-Mullem, Netherlands.

Fig. 1 shows examples of sensitivity profiles for two different collimator sections and the corresponding fits. The final step in the calibration involves re-sampling the projection data to produce projection reconstructions in object domain. Accounting for the system geometry, the radial position of each event is calculated. The events are then re-ordered with respect to the radial position from the centre of the FOV. The result allows for easier visual analysis of the acquired data; at this stage the data are completely corrected and ready for reconstruction.
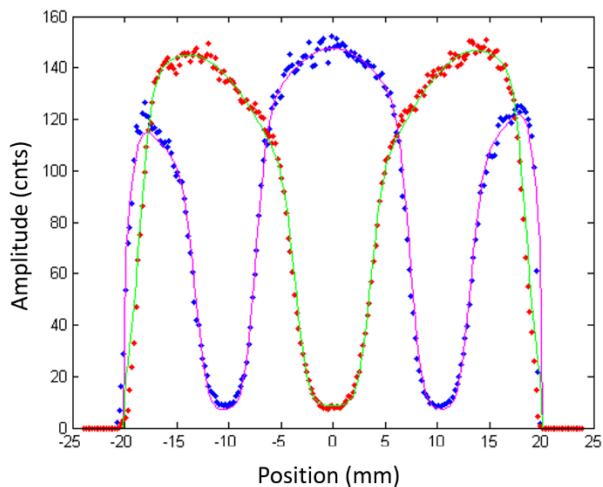

Fig. 1. Sensitivity profiles for two collimator sections and fitted analytical functions.

C. Image Reconstruction

The calibration corrected data are reconstructed using Maximum Likelihood Estimation Maximization (ML-EM), [6] in combination with angular blurring, [7]; figure 2 shows capillary phantom reconstructed in this way. The image shows promising results across the field-of-view (FOV) however the reconstruction is limited by the angular sampling of the MSS collimator and the partial ring system. We were able to overcome this by introducing a dual reconstruction of two sets of acquisition data. As an additional option, the phantom data may be acquired at two angular positions, separated by a rotation about the z-axis. The second acquisition will provide projections from the missing region of the detector ring; an offset of half a detector also provides data in between each unit and provides improved angular sampling. The increase sampling overcomes detection failure over a large area; if a large region is missing, the rotated position is able to capture events from another detector unit. The known positions of each acquisition are treated as two subsets, reconstructing both sets of data simultaneously, analogous to an ordered subset expectation maximization (OSEM) algorithm, [8]. The images were further improved with the use of structural information, simulating the use of MRI in the system. A post reconstruction partial volume correction (PVC) was carried out on the dual reconstructed images, [9].

III. RESULTS

The reconstructed capillary phantom images were used to determine the system image resolution. The trans-axial resolution was determined at various radial positions across the detector's 20x20x9 cm^3 FOV, Fig. 3. Measurements of the radial and tangential resolution show the effects of partial ring reconstruction; the bottom capillaries in Fig. 2 are in the region with no detectors and so the reconstructed values have a greater error. The system resolution is most stable closer to the centre of the FOV where the partial ring effects are less prominent. The standard deviation in resolution is greatest on the edge of the FOV where the point sources appear to stretch radially, Table I.
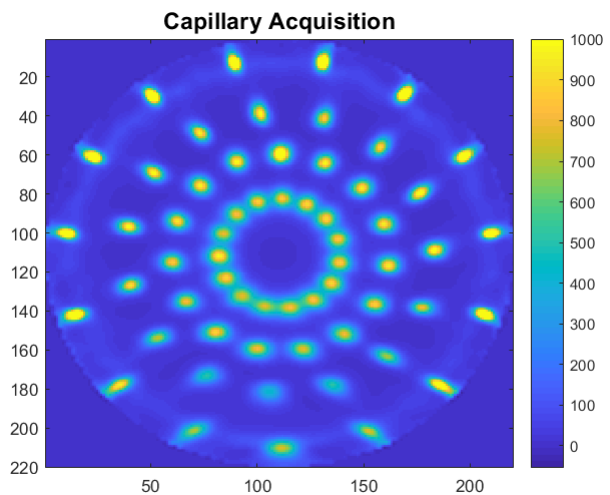

Fig. 2. The reconstructed capillary phantoms after corrections. The capillaries had 1mm diameter; each were filled with 10 MBq of ^{99m}Tc and were scanned for 5 minutes.

The phantom acquisitions include a Cold Rods phantom, a Hot Spheres phantom and a 2D Hoffman Brain phantom. Figures, 4, 5 and 6, show the results of the dual reconstruction method and the improvement from the post reconstruction PVC.

TABLE I. TRANS-AXIAL RESOLUTION

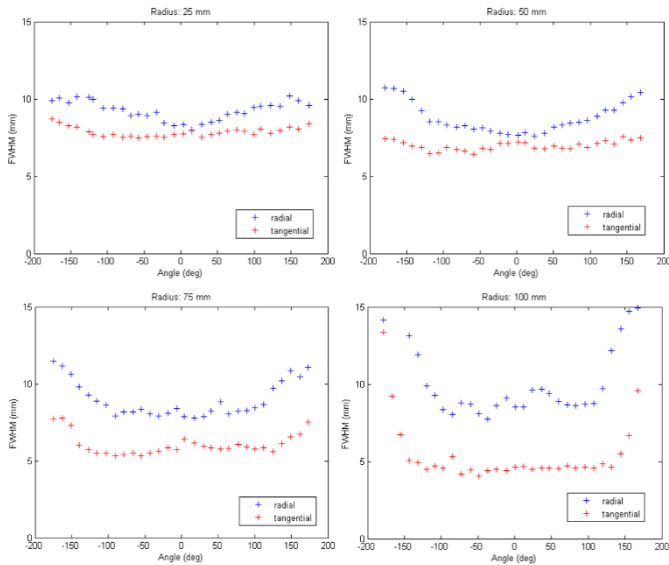| Radial Position [mm]	Mean Radial Resolution [mm]	Mean Tangential Resolution [mm]
25	9.39 ± 0.66	7.95 ± 0.51
50	8.87 ± 1.15	7.31 ± 0.25
75	9.49 ± 1.27	6.59 ± 0.95
100	8.83 ± 2.00	5.16 ± 1.08

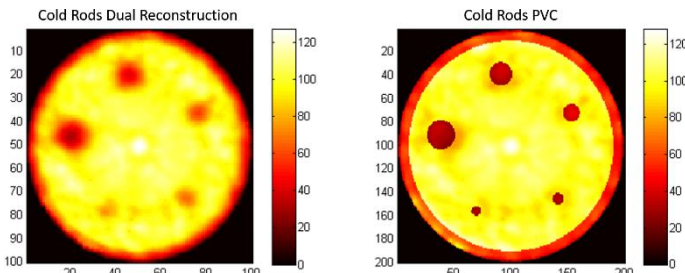Fig. 3. Resolution of capillaries at 4 radial positions against the angular position in the FOV.

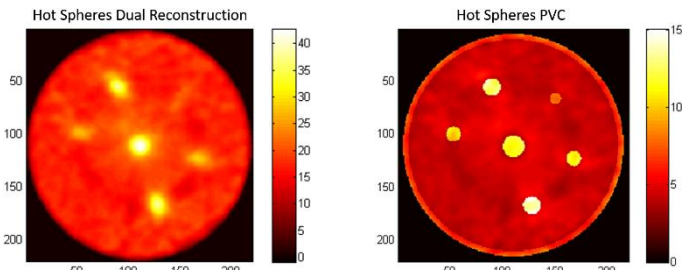Fig. 4. Cylinder phantom of 50 MBq of ^{99m}Tc and cold rods of diameters; 8, 10, 15, 20 and 25 mm.

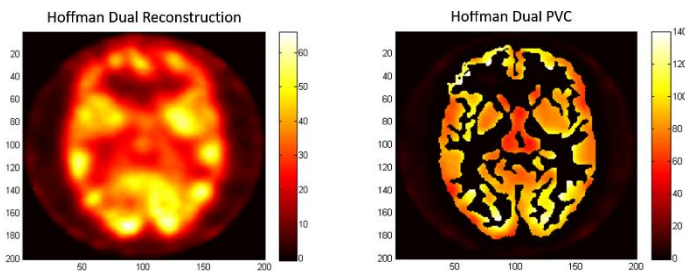Fig. 5. 60 MBq of ^{99m}Tc to a ratio of 8:1 in the hot spheres of diameters; 11, 14, 17, 21 mm.

Fig. 6. 2D Hoffman phantom with 25 MBq of ^{99m}Tc.

IV. CONCLUSION AND DISCUSSION

Overall the acquisition and reconstruction methods have demonstrated effective means of generating reconstructed images from incomplete data acquisition. We are able to correct for inhomogeneity in the detectors and produce correct projection data. The sensitivity model is able to improve image reconstruction by accounting for geometric variations across the projections. The results of this research improved the processing of INSERT projection data and introduced dual reconstruction, which can be used to benefit the system's clinical performance. The images acquired show some limitation in the system, however we are able to produce good quality images from the SPECT system alone. Implementing the dual reconstruction has shown to improve the images, however we treat this as an extension to our system, the system is able to function and produce good quality images without this step.

The INSERT detector technology has undergone preliminary characterization of the SPECT system, [10], however complete MR compatibility has only been validated in the preclinical system, [11]. Future work will set out to test the system in a clinical MR environment and to streamline calibration and acquisition procedures for routine use. The use of MR data will improve the images further and demonstrate the potential of the fully operational system.

REFERENCES

[1] D. Salvado et al., "Novel collimation for simultaneous SPECT/MRI," in 2014 IEEE (NSS/MIC) Conf. Rec., Nov. 2014, pp. 1–5. DOI: 10.1109/NSSMIC. 2014. 7430894.

[2] D. Salvado et al., "Development of a practical calibration procedure for a clinical SPECT/MRI system using a single insert prototype detector and multimini slit-slat collimator," IEEE Transactions on Radiation and Plasma Medical Sciences, vol. 2, no. 4, pp. 380–386, Jul. 2018, ISSN: 2469-7311. DOI: 10.1109/TRPMS.2018.2828163.

[3] B. Hutton et al., "Insert: A novel clinical scanner for simultaneous SPECT/MRI brain studies," in 2017 IEEE (NSS/MIC/RTSD) Conf. Rec., Oct. 2017, pp. 1–2. DOI: 10.1109/NSSMIC. 2017.8532723.

[4] V. N. Solovov et al., "Position reconstruction in a dual phase xenon scintillation detector," IEEE Transactions on Nuclear Science, vol. 59, no. 6, pp. 3286–3293, Dec. 2012, ISSN: 0018-9499. DOI: 10.1109/TNS.2012. 2221742.

[5] M. Occhipinti et al., "Light response estimation and gamma events reconstruction in gamma-detectors based on continuous scintillators and SiPMs," in 2016 IEEE (NSS/MIC/RTSD) Conf. Rec., Oct. 2016, pp. 1–4. DOI: 10.1109/NSSMIC.2016.8069405.

[6] L. A. Shepp et al., "Maximum likelihood reconstruction for emission tomography," IEEE Transactions on Medical Imaging, vol. 1, no.2, pp.113–122, Oct. 1982, ISSN:1558-254X. DOI: 10.1109/TMI. 1982.4307558.

[7] A. Bousse et al., "Angular rebinning for geometry independent SPECT reconstruction," in Conference proceedings of the 2013 Meeting on Fully Three-dimensional reconstruction in radiology and nuclear medicine, 2013.

[8] H. M. Hudson et al., "Accelerated image reconstruction using ordered subsets of projection data," IEEE Transactions on Medical Imaging, vol. 13, no. 4, pp. 601–609, Dec. 1994, ISSN: 1558-254X. DOI: 10.1109/42.363108.

[9] K. Erlandsson et al., "A review of partial volume correction techniques for emission tomography and their applications in neurology, cardiology and oncology," Physics in Medicine and Biology, vol. 57, no. 21, R119–R159, Oct. 2012. DOI: 10 .1088/0031-9155/57/21/r119.

[10] M. Carminati et al., "Clinical SiPM-based MRI-compatible SPECT: Preliminary characterization," IEEE Transactions on Radiation and Plasma Medical Sciences, pp. 1–1, 2019, ISSN: 2469-7303. DOI: 10.1109/TRPMS.2019.2951355.

[11] M. Carminati et al., "Validation and performance assessment of a preclinical SiPM-based SPECT/MRI insert," IEEE Transactions on Radiation and Plasma Medical Sciences, vol. 3, no. 4, pp. 483–490, Jul. 2019, ISSN: 2469-7303. DOI: 10. 1109/TRPMS.2019.2893377.